Fundamental limit to the use of effective medium theories in optics

Graham Hugh Cross

University of Durham, Department of Physics, Durham DH1 3LE, UK (g.h.cross@durham.ac.uk)

Received May 10, 2013; revised July 3, 2013; accepted July 16, 2013;
posted July 17, 2013 (Doc. ID 189959); published August 8, 2013

The effective medium refractive index of a surface-bound submonolayer of polystyrene nanospheres in water is found to be ill-defined below a rather specific sphere occupied area limit. The submonolayer takes on a recognizable thickness and refractive index only when the average center separation between spheres is at or below the inverse of the wavenumber. An anticipated limit to the Maxwell Garnett theory is therefore confirmed. It is proposed that this reveals a fundamental property of light scattering that is not of the Huygens spherical secondary wave type.

OCIS codes: (260.2065) Effective medium theory; (260.2710) Inhomogeneous optical media; (130.6010) Sensors.
http://dx.doi.org/10.1364/OL.38.003057

The refractive index for colloidal or otherwise multicomponent optical media is described in terms of some form of effective medium theory (EMT). This takes the optical properties of the constituents (the "continuous" and the "discontinuous" phases) and assumes the light to extend spatially and have sufficiently long wavelength so that the induced local current densities at the locations of the discontinuous phase may be considered spatially averaged. This is the textbook "mean-field" approach allowing Maxwell's equations to refer to macroscopic constitutive properties [1].

These assumptions lead to a very simple idea: the constitutive property of interest (refractive index in this case) will be measured approximately to be the volume fraction (f_V) averaged refractive index of the bulk values of the constituents. A simple illustrative constitutive law is $n_{\mathrm{eff}}^{\mathrm{EMT}} = f_V n_{\mathrm{sp}} + (1 - f_V) n_m$, where n_{sp} and n_m are the bulk values of (for example, as the discontinuous phase) latex nanospheres [2] and surrounding medium (water), respectively. This trend holds even for theories that take account of higher order Mie resonances for large spherical particles (those where the diameter is a fair fraction of the effective wavelength) [3]. These "extended" EMTs still require $n_{\mathrm{eff}}^{\mathrm{EMT}} \propto f_V$ and that is what would be expected in an experiment. However, in nanocomposites, this simple proportionality is not always strictly observed [4] and anomalous effective medium refractive indices have also been seen for sparse gold nanoparticle layers [5]. There has also been a proposal [6] that large period subwavelength 2D gratings, where EMTs are often applied, may not legitimately be described by an effective homogeneous medium at all. These situations may be those where the assumptions no longer apply, but it shows that some clarification in this area is needed.

The problem therefore to be tested here is that of knowing when to treat a sparse surface distribution of nanoparticles as a continuous layer having a well-defined thickness and refractive index. Because the nanosphere diameters in the present work are much smaller than the effective wavelength and furthermore, the refractive index contrast between them and the surrounding medium is relatively low, no anomalous scattering behavior [7] is expected. The particles are effectively Rayleigh (point-like dipole) scatterers. In these circumstances, all EMTs, including the extended theories, converge onto a "long wavelength" limit and become equivalent to simple constitutive descriptions such as that given earlier. For a two-component inhomogeneous effective medium comprising spheres of relative permittivity, $\varepsilon_{\mathrm{sp}}$ embedded in a "continuous" medium with permittivity ε_m at (for a layer system [8]) an area fractional occupied density f_A, the Maxwell Garnett (MG) model [9] is a valid model to consider

$$\frac{(\varepsilon_{\mathrm{eff}} - \varepsilon_m)}{(\varepsilon_{\mathrm{eff}} + 2\varepsilon_m)} = f_A \frac{(\varepsilon_{\mathrm{sp}} - \varepsilon_m)}{(\varepsilon_{\mathrm{sp}} + 2\varepsilon_m)}. \tag{1}$$

The effective relative permittivity $\varepsilon_{\mathrm{eff}}$ directly provides the effective medium refractive index through $n_{\mathrm{eff}}^{\mathrm{EMT}} = \sqrt{\varepsilon_{\mathrm{eff}}}$ provided that the material components are free of magnetic current densities. This expression approximately follows the linear proportionality $n_{\mathrm{eff}}^{\mathrm{EMT}} \propto f_A$ over a satisfactorily large range of area occupied fractions. However, MG himself was clear that Eq. (1) would only apply correctly for Rayleigh scattering systems when there are "many spheres to a wavelength (*sic*) of light in the medium" [9]. The question is: How many is sufficient?

For spheres in a layer, the (slightly modified) Wigner–Seitz method [10] gives the average nanosphere center–center separation, $\langle S \rangle$ according to $\langle S \rangle = \sqrt{\mathrm{FF}} \times 2r_{\mathrm{sp}}/\sqrt{f_A}$, where r_{sp} is the sphere radius and *FF* is a "fill factor" that represents the sphere area maximum packing limits and will be a number between $\pi/4$ (square close packed) and $\pi/2\sqrt{3}$ (hexagonal close packed, HCP), depending on the presence of any structural order. Here, we choose an intermediate value (FF = 0.85) in the absence of any anticipated order. Substitution into Eq. (1) then gives a method of determining the average sphere separation from $n_{\mathrm{eff}}^{\mathrm{EMT}}$. This is accurately measurable, in principle, using dual polarization interferometry (DPI).

DPI is being used by a wide range of bio-scientists and surface scientists to elucidate the thickness and density of ultrathin layers [11,12]. However, it is limited to providing the thickness and refractive index of "equivalent" continuous layers. Even though a layer may comprise sparsely distributed particles, the thickness and refractive index values obtained are merely solutions

to the multilayer dielectric continuum electrodynamic (CE) model that takes the experimental data (phase retardations and sample length) and finds a uniform layer model that fits the data. In many experiments, when looking at data where it is known that a sparse matter field distribution has been attached to the surface, some consistently observed anomalies in the interpreted layer properties are found [13,14]. These problems become self-evident when attempts to calibrate the whole technique using nanoscale dielectric spherical particles of very well-known dimensions and refractive index fail in the dilute matter field limit [15]. In particular, the layer thickness is always underestimated in the dilute limit and, as will be shown here, this is as a result of an anomalous overestimation of the equivalent layer refractive index.

In DPI, light from the TEM_{00} mode of a 20 mW helium neon laser is expanded by a Powell lens to bathe the entire end face (approx. 5.8 mm × 0.4 mm) of the dual slab waveguide sensor chip and excite the single slab waveguide modes in the upper and lower guides (with effective wavelength $\lambda_{\text{eff}} \approx 420$ nm in this experiment). The input power coupling efficiency to each waveguide is estimated to be around –26 dB. The input light polarization state is actively switched between transverse electric (TE) and transverse magnetic (TM) excitation conditions by a liquid crystal wave plate at 50 Hz. The output far-field Young's fringe pattern formed from the slab waveguide modes then provides, by Fourier transformation, the accumulated real-time (during the deposition of the layer) mode field phase changes, $\Delta\phi_{\text{TE}}$ and $\Delta\phi_{\text{TM}}$. These are used to calculate solutions to Maxwell's equations for a one-dimensional multidielectric layer CE model [16] that finds the effective medium refractive index, $n_{\text{eff}}^{\text{EMT}}$ and thickness, t of the surface bound equivalent layer.

CE multilayer modeling [17] can also be used to obtain a model sphere separation prediction. By fixing an expected maximum layer thickness, the linear relationship between $\Delta\phi_{\text{TE}}$ and an equivalent layer effective medium index can be found. Equation (1) and the Wigner–Seitz relationship then predict the average separation expected for the measured $\Delta\phi_{\text{TE}}$. This simple unrestricted "long wavelength" MG model predicts that the waveguide mode phase velocity would linearly decrease ($\Delta\phi_{\text{TE}}$ increase) as area fraction of spheres (and thus $n_{\text{eff}}^{\text{EMT}}$) linearly increases and that $\langle S \rangle$ accordingly would decrease monotonically, during the deposition.

Experimentally, the sample ("upper") slab waveguide thickness and refractive index is first calibrated in the instrument using a bulk medium exchange between pure water and 80% (v/v) ethanol in water, the refractive indices of which are well known. Polystyrene sphere suspensions (in water, 2 mM azide) of 2% weight/volume (FluoSpheres carboxylate-modified, Molecular Probes, Oregon, USA) in aliquots of 200 μl, are diluted with 3.8 ml pure phosphate buffer solution and introduced to the sample injection loop system. Full sample exchange occurs over around 4 s. The chip surface is functionalized with amine groups, and spheres attach to the surface by electrostatic attraction, the strength of which can be controlled by varying the pH value of the flow medium.

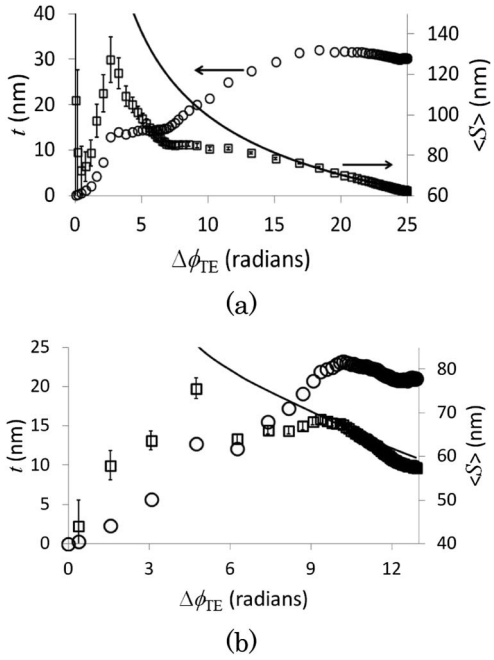

Fig. 1. (a) Deduced layer thickness (circles) and average separation (squares) versus TE mode phase retardation for the deposition of (nominally) 30 nm diameter polystyrene spheres, MG model $\langle S \rangle$ shown for comparison (solid line). Data points represent sample time intervals of 1 s. Error bars are calculated using the phase retardation random noise 5σ uncertainty of ±5 mrad and ±3 mrad, for $\Delta\phi_{\text{TE}}$ and $\Delta\phi_{\text{TM}}$, respectively averaged over a total pre-deposition time of 120 s. (b) Data from a sphere deposition experiment using (nominally) 21 nm diameter spheres [symbols and error methods as for (a)].

The results of two typical deposition experiments are presented in Figs. 1(a) and 1(b) for 30 and 20 nm (nominal diameters), respectively. We are looking for a convergence condition with the MG theory. The failure above some critical predicted average sphere separation is clear. Above the sphere separation region of convergence the layer thickness is underestimated. The CE model has to find an equivalent layer solution that matches the (anomalously high) refractive indices at the (relatively low) phase retardations prevailing. It thus solves for a low layer thickness. It is important here to note that the layer effective index is linearly related to the measured ratio of the retardations, $R = \Delta\phi_{\text{TE}}/\Delta\phi_{\text{TM}}$ irrespective of their magnitudes. The distinguishing feature of the DPI technique is that it measures the layer refractive index as a manifestation of the waveguide mode dispersion differences between the TE and TM modes. This is different from conventional interferometry methods that would make the naive assumption that refractive index can be deduced directly from the phase retardation over a known length of material. It is this feature that gives the technique the ability to identify phase path types through the media, to be discussed shortly.

Convergence between the measured and theoretical average sphere separation occurs when $\langle S \rangle \approx 67$ nm and, for 30 nm spheres, at $\Delta\phi_{\text{TE,30}} \approx 22$ radians, just after the point where the CE model layer thickness (~31 nm) corresponds to the sphere diameter. The CE model effective medium refractive index ($n_{\text{eff}}^{\text{EMT}} = 1.382$) is taken as correct at this point and one can therefore confidently

use Eq. (1) to obtain a critical area occupied density $f_{A,C} \approx 0.2$. This behavior is repeated ($\langle S \rangle \approx 67$ nm, $\Delta\phi_{\mathrm{TE},20} \approx 10$ radians) when the corresponding experiment is undertaken with 20 nm spheres (Fig. 2). Thus we would say that Maxwell Garnett's "many spheres to a wavelength" requirement, echoed by Bohren [18], is $420/67 \sim 6$ in this case.

Further confirmation that $f_{A,C}$ correlates correctly with $\Delta\phi_{\mathrm{TE}}$ at the convergence point is found from the ratio of squared radii that equals the ratio of retardations at this point, that is, $r_{30}^2/r_{20}^2 \approx \Delta\phi_{\mathrm{TE},30}/\Delta\phi_{\mathrm{TE},20} \approx 2.2$.

The lack of rationale for what we will henceforth refer to as "refractive index," in quotes, has been studied further in a deposition where only a very dilute, uniform, but random, layer of 100 nm diameter spheres is produced [Figs. 2(a) and 2(b)]. A 1000:1 dilution of the sphere stock suspension is passed over the chip surface to limit the deposition. Using the CE modelled linear progression of R with $\Delta\phi_{\mathrm{TE}}$ for a 100 nm equivalent uniform layer with increasing $n_{\mathrm{eff}}^{\mathrm{EMT}}$ ($R = 0.0006\Delta\phi_{\mathrm{TE}} + 0.7419$), a comparison between the CE model-predicted R and that observed can be made. The dilute layer of spheres exhibits an end-point raw data R value of 0.752 ± 0.001, which would imply a layer "refractive index" of 1.349 and from Eq. (1) an expected area occupied density $f_A \approx 0.075$. However, the observed (by SEM) average sphere separation is around 1 μm with $f_A \approx 0.01$. An overestimation of the coverage of nearly 8 times is therefore predicted by the raw data, which is evidently incorrect. Similarly, the observed coverage leads, from Eq. (1), to an effective

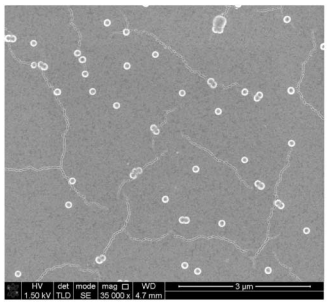

(a)

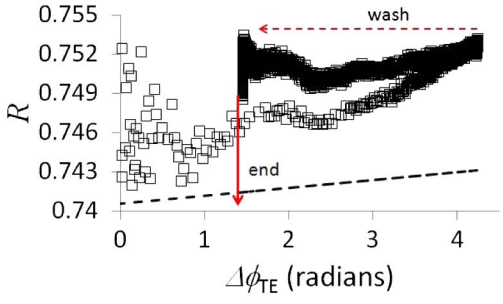

(b)

Fig. 2. (a) SEM micrograph of the surface bound 100 nm spheres. Coverage is almost uniform along the full interferometer path (see supplementary information in [25]). (b) R versus $\Delta\phi_{\mathrm{TE}}$ with error bars removed for clarity. The CE model R versus $\Delta\phi_{\mathrm{TE}}$ (for slope values, see text) is shown as the dashed line. The data range indicated by the dashed arrow and labelled "wash" represents the behavior when pure water is reintroduced to the interferometer chip.

"index" value of 1.333 so the measured "index" is also overestimated by a significant amount and cannot be regarded as a physically realistic constitutive property of this sparse layer.

If one accepts the argument that $\Delta\phi_{\mathrm{TE}}$ is broadly proportional to sphere area occupied density, then two quite striking anomalies are apparent. First, in the early stage data [below 1 radian, Fig. 2(b)] R reduces or is constant with increasing $\Delta\phi_{\mathrm{TE}}$. This, if EMT theories were assumed valid, would imply a reducing or constant refractive index (increasing $\langle S \rangle$, see Fig. 1) with increasing area occupied density of the spheres. Second, upon washing, with $\Delta\phi_{\mathrm{TE}} \approx -3$ radians and presumably removing weakly bound spheres, R remains almost constant. This further undermines the validity of the usual $n_{\mathrm{eff}}^{\mathrm{EMT}} \propto f_A$ EMT relationship.

Possible explanations for the observation of the critical sphere area density limit and the anomalous dilute limit "index" are required. Two are offered here.

First, there may be some significance in the critical sphere separation $\langle S \rangle_C$ if it is realized that it coincides with the following "correspondence" relationship

$$1/k = \lambda_{\mathrm{eff}}/2\pi = \hbar/p_M = \langle S \rangle_C, \tag{2}$$

where k is the classical effective wavenumber, p_M the de Broglie wave momentum, and λ_{eff} is the effective wavelength. One might then note a coincidence with the Ioffe–Regel condition [19] ($k\ell = 1$) for "Anderson" localization of scalar light waves [20] and suggest, following John [21], that above the matter field density point at which the mean free path, ℓ for photons (in this case the average spacing between spheres) equals the inverse wavenumber the spheres are somehow "optically connected." This could be interpreted in the spirit that the spheres and their surroundings then constitute an effective medium. Despite the intriguing possibilities for this, in the present work, where $\lambda/r_{\mathrm{sp}} \gg 1$ and the permittivity contrast $\varepsilon_{\mathrm{sp}}/\varepsilon_m \approx 1.4$, the effective scattering cross section of spheres is vanishingly small and in the Rayleigh range, and it clearly represents a "weak" scattering situation. The conventional view is that phenomena revealing localization of photons, by contrast, require "strong" scattering as in the observation of delayed photons emerging from compressed titania-in-air nanosphere samples [22].

Second, the propagation model of Huygens may require revisiting [23]. Spreading secondary wavelets are the conventional basis of propagation models for "point-source" multiple scattering media [24], but these lead to long wavelength EMTs that fail to describe the present system. A detailed alternative hypothesis for this is offered [25], which, in brief, comprises the idea that the measured ratios are phase-path averaged values, $\bar{R}$. Light rays following tortuous ray eikonals accumulate phase path retardation in ratios of two basic types, present in varying proportions depending on the morphology and density of the system. One is a refractive type, R_r, with values ranging linearly between around 0.74 (dilute) and 0.80 (dense) in accordance with a local "ray-area" effective medium response. The suggestion is that the ray's field is averaging the induced current densities only over a limited transverse area. The other is a geometrical

type, R_g, independent of the effective medium response and thus polarization independent. This represents light following "off-axis," nonballistic, ray paths. Phase retardation accumulates on these paths without influence from the mode field dispersion effect (i.e., paths where the surface is free of bound spheres or where the ray cannot "see" them). These geometrical paths can only make contributions $R_g = \Delta\phi_{\mathrm{TE}}/\Delta\phi_{\mathrm{TM}} = 1$ in some proportion to the total path-averaged value. These contributions enhance the measured $\bar{R}$ values when off-axis scattering is most prevalent (ultradilute, inhomogeneous layer distributions) and give rise to an anomalously high "refractive index." At the critical area fraction, the proportion of R_g paths tends to zero (off-axis scattering is extinguished) and all the rays then follow ballistic trajectories. A system resembling a homogeneous optical medium then emerges and the EMT model works.

The photon/ray paths are presumably Fermat's "paths of least time," akin to "paths of least action" [26]. These accumulate phase retardations characteristic of the delayed photons purportedly seen in [22] but with photon excess retardations (delays) presumably somewhat smaller in this weak scattering situation.

The 20 and 30 nm sphere data were kindly provided by Marcus Swann of Biolin Scientific. 100 nm sphere SEM image by L. Bowen, Durham G. J. Russell Microscopy Facility. I thank S. Brand for insightful discussions on this work and J. Girkin and D. Bloor for critical reading of the draft manuscripts.

References and Notes

1. G. Brooker, *Modern Classical Optics* (OUP, 2002).
2. R. E. Miles, S. Rudić, A. J. Orr-Ewing, and J. P. Reid, J. Phys. Chem. A **114**, 7077 (2010).
3. R. G. Barrera, A. Reyes-Coronado, and A. Garcia-Valenzuela, Phys. Rev. B **75**, 84202 (2007).
4. N. Sergienko, D. Godovsky, B. Zavin, M. Lee, and M. Ko, Nanoscale Res. Lett. **7**, 181 (2012).
5. M. Chen and R. G. Horn, J. Colloid Interface Sci. **315**, 814 (2007).
6. P. Lalanne and D. Lemercier-lalanne, J. Mod. Opt. **43**, 2063 (1996).
7. C. Yang, A. Wax, and M. S. Feld, Opt. Lett. **26**, 235 (2001).
8. R. H. Doremus, J. Appl. Phys. **37**, 2775 (1966).
9. J. C. Maxwell-Garnett, Phil. Trans. R. Soc. A **203**, 385 (1904).
10. L. A. Girifalco, *Statistical Mechanics of Solids* (OUP, 2003).
11. G. H. Cross, A. A. Reeves, S. Brand, J. F. Popplewell, M. J. Swann, and N. J. Freeman, Biosens. Bioelectron. **19**, 383 (2003).
12. G. H. Cross, A. A. Reeves, S. Brand, J. F. Popplewell, L. L. Peel, M. J. Swann, and N. J. Freeman, J. Phys. D **37**, 74 (2004).
13. A. W. Sonesson, T. H. Callison, H. Brismar, and U. M. Elofsson, Colloids Surf. B **54**, 236 (2007).
14. K. Xu, M. M. Ouberai, and M. E. Welland, Biomaterial. **34**, 1453 (2012).
15. G. H. Cross, N. J. Freeman, and M. J. Swann, in *Handbook of Biosensors and Biochips*, R. S. Marks, D. C. Cullen, I. Karube, C. R. Lowe, and H. H. Weetall, eds. (Wiley, 2007), Chap. 32.
16. "Resolver" is the CE multi-layer model developed for DPI.
17. SLAB v.4.0 (1-D waveguide mode solver), BBV Software.
18. C. F. Bohren, J. Atmos. Sci. **43**, 468 (1986).
19. A. F. Ioffe and A. R. Regel, in *Progress in Semiconductors*, A. F. Gibson, F A. Kroger, and R. E. Burgess, eds. (Heywood, 1960), Vol. **4**, p. 237.
20. M. P. V. Albada and A. Lagendijk, Phys. Rev. Lett. **55**, 2692 (1985).
21. S. John, Phys. Today **44**(5), 32 (1991).
22. M. Störzer, P. Gross, C. M. Aegerter, and G. Maret, Phys. Rev. Lett. **96**, 063904 (2006).
23. P. Enders, Lat. Am. J. Educ. **3**, 19 (2009).
24. V. K. Varadan, V. N. Bringi, and V. V. Varadan, Phys. Rev. B **19**, 2480 (1978).
25. G. H. Cross, http://arxiv.org/abs/1303.1390.
26. R. P. Feynman, R. B. Leighton, and M. Sands, in *The Feynman Lectures on Physics* (Addison-Wesley 1964), Vol. **1**, Chap. 26.